ISSN 0915-633X

NATIONAL INSTITUTE FOR FUSION SCIENCE

Effect of Energetic Ion Loss on ICRF Heating Efficiency and Energy Confinement Time in Heliotrons

S. Murakami, N. Nakajima, M. Okamoto and J. Nührenberg

(Received - Apr. 21.1999)

NIFS-599 June 1999

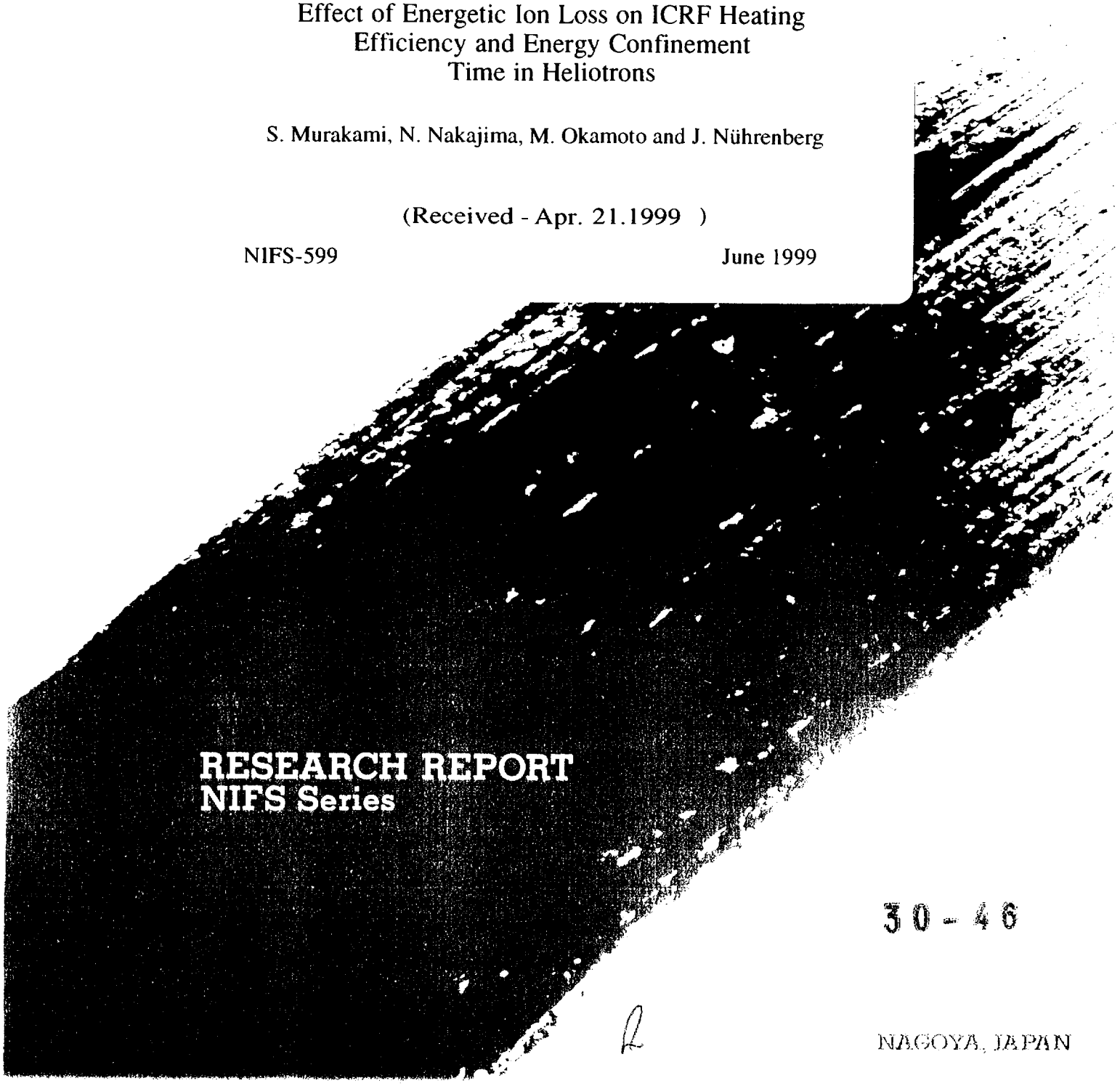

RESEARCH REPORT
NIFS Series

NAGOYA, JAPAN

Effect of Energetic Ion Loss on ICRF Heating Efficiency and Energy Confinement Time in Heliotrons

S. Murakami, N. Nakajima and M. Okamoto
National Institute for Fusion Science,
Oroshi, Toki 509-5292, Japan

J. Nührenberg
Max-Planck-Institut, Plasmaphysik,
D-17489 Greifswald, Germany

Abstract

ICRF heating efficiency and the global energy confinement time during ICRF heating are investigated including the effect of energetic ion loss in heliotrons. The approximate formula of ICRF heating efficiency is derived using the results based on Monte Carlo simulations. The global energy confinement time including energetic ion effect can be expressed in terms of ICRF heating power, plasma density, and magnetic field strength in heliotrons. Our results in the CHS plasma show the systematic decrement of the global energy confinement time due to the energetic ion loss from the assumed energy confinement scaling law, which is consistent with the experimental observations. Also we apply our model to the ICRF minority heating in the LHD plasma in two cases of typical magnetic configurations. The clear increment of the global energy confinement time due to the stored energy of energetic tail ions is obtained in the "orbit improved" configuration, while the decrement is observed in the "standard" configuration.

Keywords: ICRF heating, energetic ion, orbit loss, global energy confinement, heliotron

1 Introduction

Recent experiments of ion cyclotron range of frequency (ICRF) heating in helical systems[1-7] have demonstrated the effectiveness of this heating method in non-axisymmetric configurations. Especially the successes of the long time operations[5,6] have shown the importance of ICRF heating for future steady state operations in helical systems. In these experiments highly energetic tail ions (up to several hundreds keV) have been observed due to the acceleration by ICRF waves. The higher energetic tail ions (up to MeV order) will be generated in future experiments of non-axisymmetric devices (LHD and W7-X).

The stored energy of energetic ion tail increases the total stored energy effectively and this increment of the stored energy could contribute to the global energy confinement of plasma. Previous ICRF heating experiments in tokamaks have shown the certain increment of energy confinement due to energetic ions during the ICRF heating[8] and combining heating with NBI[9,10]. However, the experimental results in the Compact Helical System (CHS; $l = 2$, $m = 8$, heliotron) have shown that the global energy confinement time of ICRF heating plasma is systematically lower than both that of NBI heating plasma and the value estimated by the LHD scaling law[11].

The ICRF heating increases the ion energy perpendicular to the magnetic field line and generates the energetic ripple trapped ions in heliotrons. The behaviors of these ripple trapped ions are complicated and have large orbit size in the radial direction. Therefore

the energetic ions due to ICRF heating tend to diffuse radially and would be finally lost by orbit loss. In the previous papers[12-14] we have studied the drift orbit effect of energetic ions on the ICRF heating in heliotrons using the Monte Calro simulation code, where complicated orbits of energetic ions, Coulomb collisions, and interaction between the particles and applied RF wave are included. It has been shown that the energetic ripple trapped ions are generated by ICRF heating and significant fraction of energetic ions are lost by energetic ion orbit loss when the ICRF heating power increases more than 10MW.

So the inclusion of energetic ion orbit loss is necessary in considering the ICRF heating in heliotrons. The orbit loss of energetic ions leads to the power loss and deteriorates the energy confinement of plasma. The previous Fokker-Planck analysis assuming simple orbit loss model[15] pointed out the apprehension of decrement of the global energy confinement due to the energetic ions loss. Because of complicated drift motions of energetic ions, the more realistic model including the orbit effect in a three dimensional magnetic configuration is required to explain and predict experimental results in heliotrons.

In this paper we study the ICRF heating efficiency and the global energy confinement time including the effect of energetic ion loss in heliotrons. The confinement of energetic tail ions is assumed to be expressed by the slowing down time and the heating efficiency (=the power transferred to the bulk plasma from ICRF heated energetic ions / the power absorbed to energetic ions from ICRF wave). The power loss by energetic ion orbit loss is modeled based on the Monte Carlo simulation results and the approximate formula of the heating efficiency is derived. Combining the obtained heating efficiency with the energy confinement time of bulk plasma, the global energy confinement time is expressed in terms of heating power, plasma density, and magnetic field strength.

In section 2, we first derive the global energy confinement time including the effects of energetic ion on the heating efficiency. The heating efficiency model is considered starting from the power balance of ICRF heated energetic ions. Finally the global energy confinement time is obtained as a function of the density, temperature, and magnetic field strength. In section 3 we study the effect of high energy ion loss on the global energy confinement time in the CHS plasma. Next we apply that to the ICRF minority heating for the Large Helical Device (LHD; $l = 2$, $m = 10$ heliotron)[16] introducing two typical configurations; "standard" configuration and "orbit improved" configuration in section 4. Conclusions are given in Section 5.

2 ICRF Heating Efficiency and Energy Confinement Time

2.1 Energetic ion effect on energy confinement time

A launched ICRF wave generates the energetic ion tail distribution and the input ICRF power is first stored in the energetic tail ions. Then, the stored energy in the energetic ions is transferred to the bulk plasma through particle collisions (slowing down process). Here, we consider that the total stored energy, W_{tot}, consists of two parts; one is the stored energy of the bulk plasma, W_{bulk}, and the other is the stored energy of energetic tail ions, W_{tail}, as

$$W_{tot} = W_{bulk} + W_{tail}. \tag{1}$$

These stored energies can be expressed by

$$W_{tot} = P_{total}\tau_E^{glb}, \tag{2}$$

$$W_{tail} = P_{abs}\tau_E^{tail}, \tag{3}$$

$$W_{bulk} = P_{trns}\tau_E^{bulk}, \tag{4}$$

where P_{total}, P_{abs} and P_{trns} are the total plasma heating power, the absorbed power of energetic tail ions from ICRF wave, and the transferred power from energetic tail ions to bulk plasma, respectively. In Eqs. (2) to (4), τ_E^{glb}, τ_E^{bulk} and τ_E^{tail} are the global energy confinement time, the energy confinement time for bulk

plasma and for energetic tail ions, respectively. Note that the difference between P_{abs} and P_{trns} corresponds to the power loss by the energetic ions and that we consider the orbit loss as a dominant loss mechanism in this paper.

The stored energy of energetic tail ions is transferred to bulk plasma due to the slowing down process and the transferred power is approximately expressed as $P_{trns} = W_{tail}/(\tau_s/2)$, where τ_s is the slowing down time for tail ions ($dv/dt = -\tau_s^{-1}v$). Using this relation and Eq. (3) the energy confinement time of tail ions is given by

$$\begin{aligned} \tau_E^{tail} &= \frac{W_{tail}}{P_{abs}}, \\ &= \eta\tau_s/2, \end{aligned} \tag{5}$$

where $\eta(= P_{trns}/P_{abs})$ is the heating efficiency of ICRF heating, which corresponds to the fraction of the transferred power to the deposited ICRF heating power.

Assuming $P_{total} = P_{abs}$, the global energy confinement time is given by

$$\begin{aligned} \tau_E^{glb} &= W_{tot}/P_{abs}, \\ &= \eta(\tau_E^{bulk} + \tau_s/2). \end{aligned} \tag{6}$$

Equation (6) is a simple formula of energy confinement time including both the effect of the stored energy of the tail ions and their losses. This can be rewritten as

$$\tau_E^{glb} = \tau_E^{bulk} + \eta\tau_s/2 - (1-\eta)\tau_E^{bulk}. \tag{7}$$

The second term of right hand side shows the increment of the energy confinement time due to the stored energy of the energetic tail ions and third term is the decrement due to the power loss by energetic ion orbit loss. Also Eq. (7) gives a condition for the heating efficiency to increase the global energy confinement time due to energetic ions effect as

$$\eta \geq \frac{1}{1+\tau_s/2\tau_E^{bulk}}. \tag{8}$$

2.2 Consistent heating efficiency and energy confinement time

Next we consider the heating efficiency starting from the power balance of energetic ions including the effect of orbit loss of energetic ions. The power balance for the ICRF heated energetic ions is simply given by

$$\begin{aligned} P_{abs} &= P_{trns} + P_{loss}, \\ &= \frac{W_{tail}}{\tau_s/2} + \frac{W_{tail}}{\tau_c}, \end{aligned} \tag{9}$$

where P_{loss} is the power loss due to the orbit loss of energetic tail ions and τ_c is the particle confinement time for tail ions. Then the heating efficiency becomes

$$\begin{aligned} \eta &= \frac{P_{trns}}{P_{abs}}, \\ &= \frac{1}{1+\tau_s/2\tau_c}. \end{aligned} \tag{10}$$

In the previous Monte Carlo simulations for ICRF heating in heliotrons[13,17] we have evaluated the heating efficiency as a function of heating power and we have obtained a simple relation between the heating efficiency and input power based on Eq. (10) as

$$\eta = \frac{1}{1+P_{abs}/P_0}, \tag{11}$$

where P_0 is a function of T, B, n, ... etc., and is the value of P_{abs} when $\eta = 0.5$. Further, we generalize the heating efficiency as

$$\eta = \frac{1}{1+CP_{abs}^{\alpha}T_e^{\beta}n^{-\gamma}B^{-\delta}}, \tag{12}$$

where P_{abs}, T_e, n and B are the absorbed power from RF wave [MW], the averaged electron temperature [keV], the averaged plasma density [$10^{20}\mathrm{m}^{-3}$] and magnetic field strength [T], respectively. Since the energy range of the energetic ions is much larger than the critical energy, $E_c(\sim 15T_e$ for proton ions), and the slowing down process mainly depend on the electron temperature, the ion temperature dependency is ignored in this formula.

The Monte Calro simulations results[13,17] shows that the factor C strongly depends on the configurations, but the power factors of α, β, γ and δ weakly depend on the configurations. The power factors α,

β, γ, and δ are the positive numbers at order of unity. We have estimated the power factors from simulation results as $\alpha \simeq 1$, $\beta \simeq 2$, $\gamma \simeq 2$, and $\delta \simeq 1$, where the fraction of minority ion density to the bulk plasma density is fixed in changing the bulk plasma density.

Assuming that the bulk plasma is mainly heated by the transferred power from energetic tail ions, the electron temperature can be expressed as

$$T_e = \frac{1}{3}\frac{\tau_E^{bulk} P_{trns}}{nV_{tot}}, \tag{13}$$

where V_{tot} is the total plasma volume and we assume the same temperature for electrons and ions. Therefore, in order to evaluated the heating efficiency and temperature we must solve the coupled equations (12) and (13). Then, the relation between the heating efficiency and P_{abs} is given by

$$\begin{aligned} &\eta\{1 + C'' n^{\beta(\epsilon-1)-\gamma} B^{\beta\sigma-\delta} \\ &\times {P_{abs}}^{\alpha+\beta(1-\lambda)} \eta^{\beta(1-\lambda)}\} - 1 \;=\; 0, \end{aligned} \tag{14}$$

where $C'' = C(C'/3V_{tot})^{\beta}$ and we assume $\tau_E^{bulk} = C' n^{\epsilon} B^{\sigma} P_{trns}^{-\lambda}$, where the values of ϵ, σ, and λ are estimated from the usual energy confinement scaling law (e.g. the LHD scaling law).

Solving Eq. (14) we can obtain the heating efficiency. The slowing down time can be evaluated using the obtained electron temperature as $\tau_s = k n^{-1} T_e^{3/2}$. Then we can evaluate the global confinement time from Eq. (6) as

$$\begin{aligned} \tau_E^{glb} \;=\; &\eta\{C' n^{\epsilon} B^{\sigma} (\eta P_{abs})^{-\lambda} \\ &+ \tfrac{k}{2} (\tfrac{C'}{3V_{tot}})^{\frac{3}{2}} n^{\frac{1}{2}(3\epsilon-5)} B^{\frac{3}{2}\sigma} (\eta P_{abs})^{\frac{3}{2}(1-\lambda)}\}. \end{aligned} \tag{15}$$

The ratio between the energy confinement time with and without tail becomes

$$\begin{aligned} \tau_E^{glb}/\tau_E^{notail} \;=\; &\eta\{\eta^{-\lambda} + \tfrac{k}{2} (\tfrac{C'}{27V_{tot}^3})^{\frac{1}{2}} n^{\frac{1}{2}(\epsilon-5)} B^{\frac{1}{2}\sigma} \\ &\times P^{\frac{1}{2}(3-\lambda)} \eta^{\frac{3}{2}(1-\lambda)}\}. \end{aligned} \tag{16}$$

In the limit of the high efficient heating ($\eta \sim 1$) this ratio becomes

$$\tau_E^{glb}/\tau_E^{notail} = 1 + \frac{k'}{2} (\frac{C'}{27V_{tot}^3})^{\frac{1}{2}} n^{\frac{1}{2}(\epsilon-5)} B^{\frac{1}{2}\sigma} P^{\frac{1}{2}(3-\lambda)}.$$

It is found that energy confinement time is improved due to tail distribution and this improvement strongly depends on the density and heating power. The strong improvement can be observed in the low density and high power heating cases.

We can easily extent Eq. (15) to the situation with other heating methods, *e.g.* NBI (neutral beam injection) heating, electron direct heating by ICRF heating and ECRH (electron cyclotron resonance heating). In this case τ_E^{glb} is given by

$$\tau_E^{glb} = \tau_E^{bulk} + \frac{\eta P_{abs} \tau_s/2 - (1-\eta) P_{abs} \tau_E^{bulk}}{P_{abs} + P'}, \tag{17}$$

where P' is the heating power of additional heating and the energy confinement time of bulk plasma is $\tau_E^{bulk} = C' n^{\epsilon} B^{\sigma} (P_{trns} + P')^{-\lambda}$. Then, the heating efficiency becomes

$$\begin{aligned} &\eta\{1 + C'' n^{\beta(\epsilon-1)-\gamma} B^{\beta\sigma-\delta} \\ &\times {P_{abs}}^{\alpha} (\eta P_{abs} + P')^{\beta(1-\lambda)}\} - 1 \;=\; 0, \end{aligned} \tag{18}$$

and the final results are obtained as

$$\begin{aligned} \tau_E^{glb} \;=\; &\eta\{C' n^{\epsilon} B^{\sigma} (\eta P_{abs} + P')^{-\lambda} \\ &+ \tfrac{k}{2} (\tfrac{C'}{3V_{tot}})^{\frac{3}{2}} n^{\frac{1}{2}(3\epsilon-5)} B^{\frac{3}{2}\sigma} (\eta P_{abs} + P')^{\frac{3}{2}(1-\lambda)}\}. \end{aligned} \tag{19}$$

3 Effect on energy confinement in CHS

We apply our model to the CHS plasma and study the effect of ICRF heated energetic ions on the global energy confinement time in CHS. From the results of previous Monte Carlo simulations[13], we have estimated the power factors in the heating efficiency of Eq. (12) as $\alpha \simeq 1$, $\beta \simeq 2$, $\gamma \simeq 2$ and $\delta \simeq 1$, as mentioned in section 2.2. The constant C has been obtained as $C = 9.1$ for the CHS plasma ($R_{ax} = 0.921$m), where we assumed proton minority ions (10 %) in deuteron plasma. The LHD scaling for energy confinement time[11],

$$\tau_E^{LHD} = 0.17 R^{0.75} a^2 n^{0.69} B^{0.84} P_h^{-0.58}, \tag{20}$$

is used for the energy confinement time of bulk plasma, where R, a, n, B, and P_h are the major radius [m], minor radius [m], density [10^{20}m^{-3}], magnetic field strength [T], and injected power [MW], respectively.

Figure 1 shows (a) the ICRF heating efficiency, (b) the stored energies and (c) the electron temperature as a function of ICRF heating power with three different densities $n = 0.2$, 0.4 and $0.6 \times 10^{20}\mathrm{m}^{-3}$. The magnetic field strength is set to be $B = 0.9\mathrm{T}$ in the following simulations for CHS. It is found in Fig. 1-(a) that the heating efficiency decreases with heating power for all density cases. As heating power is increased, the more energetic ions are generated, leading to more energetic ion loss and more reduced heating efficiency. We can also see that the heating efficiency strongly depends on plasma density. This is because that the slowing down time of energetic ion becomes longer for a lower density case and that the more energetic ions are generated in the lower density case.

Fig. 1-(b) shows the plots of the total stored energy and the stored energy of bulk plasma for three different densities. The difference between these stored energies corresponds to the stored energy of energetic tail ions. Since the heating efficiency decreases with the heating power, the saturations of total stored energy can be seen in the higher heating power region. Also, the saturation occurs at a relatively lower heating power in the lower density cases, because of the lower heating efficiency. The stored energy in the energetic tail ions is about 20%. The achieved temperature also saturated around 300-400eV in the CHS in Fig. 1-(c). This saturation also occurs at lower heating power for lower density case.

The global energy confinement time with ICRF heated plasma (solid line) and the energy confinement time without ion tail effect (dashed line) in CHS are shown in Fig. 2 with the slowing down time (dotted line). The plasma density is $n = 0.6 \times 10^{20}\mathrm{m}^{-3}$. Although, a slight increment of the global energy confinement time due to the tail effect appears in the region $P \leq$ 0.2MW, the decrement of the global energy confinement time is significant in the higher heating power region. This decrement comes from the low heating efficiency in the higher power region (See Fig. 1-(a)).

Finally we compare our results with the experimental results of CHS[1]. We assumed the similar plasma parameters with CHS experiment and compared the tendency of the global energy confinement time. Figure 3 plots the obtained global energy confinement time versus the energy confinement time of LHD scaling. In the CHS experiments the direct electron heating also occurs in ICRF heating[2]. So we, here, examine the following four parameters cases by changing the heating scenario (ion heating and direct electron heating) and plasma densities; (A) only ion heating at $n = 0.15 \times 10^{20}\mathrm{m}^{-3}$, (B) ion and direct electron heating with equal weight at $n = 0.15 \times 10^{20}\mathrm{m}^{-3}$, (C) only ion heating at $n = 0.4 \times 10^{20}\mathrm{m}^{-3}$, and (D) ion and direct electron heating with equal weight at $n = 0.4 \times 10^{20}\mathrm{m}^{-3}$. Here we assume that no heating power loss occurs in the direct electron heating.

It is clearly shown that the obtained global energy confinement time is systematically lower than that of the LHD scaling law. Also the global energy confinement time is closed to that of LHD scaling in the case that the ion and direct electron heating coexist with equal weight. These tendencies well agree with the experimental observations. Therefore, our results show the important role of the power loss by the energetic ion orbit loss in the global energy confinement in the ICRF experiments of CHS.

4 Effect on energy confinement in LHD

We, next, apply our model to the LHD plasma in two cases of typical magnetic configurations. By controlling the current of the vertical coils the magnetic axis position can be horizontally shifted in the LHD and various types of configurations can be obtained. We, here, consider two configurations with different values of the magnetic axis shift. The first one is a configuration where the magnetic axis is shifted by 15cm inwardly from the center of two helical coils in vacuum. This configuration is called "standard" configuration satisfying the requirements for highly balanced plasma performance (i.e. a high plasma beta,

relatively good particle confinement, and creating a divertor configuration). The second one is a configuration where the magnetic axis is shifted by 30cm inwardly from center of two helical coils in vacuum. This configuration is called "orbit improved" configuration where the confinement of ripple trapped particle is improved drastically and the good confinement of energetic ions would be expected.

The power factors of the heating power, density, temperature, and magnetic field strength of the heating efficiency given by Eq. (12) are assumed as $\alpha \simeq 1$, $\beta \simeq 2$, $\gamma \simeq 2$ and $\delta \simeq 1$, respectively, from previous Monte Carlo simulation results[13,17]. The constant C has been obtained as $C = 0.082$ for LHD for ^{3}He minority ions (3%) in deuteron plasma. The LHD scaling for energy confinement time Eq. (20) is also used to evaluate the confinement time of bulk plasma.

The ICRF heating efficiencies in two types of LHD configurations are shown as a function of RF input power in Fig. 4; (a) the "standard" configuration and (b) the "orbit improved" configuration. Three different averaged densities $n = 0.2$, 0.4 and $0.6 \times 10^{20}\mathrm{m}^{-3}$ are used and the magnetic field strength is fixed to $B_0 = 3.0T$. It can be seen that the heating efficiency decreases as the heating power increases and that the better heating efficiencies are obtained in the "orbit improved" configuration. This is because of the improvement of energetic ion loss in the "orbit improved" configuration. The heating with the density lower than $0.4 \times 10^{20}\mathrm{m}^{-3}$ is not effective in the "standard" configuration for the heating power more than 10MW. On the other hand, the good heating efficiency is obtained even for the higher heating power in the "orbit improved" configuration.

Figure 5 shows the stored energies in the total and bulk plasma for three different plasma densities $n = 0.2$, 0.4 and $0.6 \times 10^{20}\mathrm{m}^{-3}$ in (a) the "standard" configuration and (b) the "orbit improved" configuration. The difference between the total and bulk plasma stored energy corresponds to the stored energy of the tail ions. We find that the fraction of the stored energies of the tail ions are about 10% at the heating power of 10MW in the "standard" configuration in Fig. 5-(a). That is because the obtained temperature is estimated less than 2keV at the plasma center and the estimated slowing down time is much smaller than the energy confinement time. It is also found that the maximum fraction of stored energy of the tail part is not obtained at the lowest density in the "standard" configuration, because of the low electron temperature due to the lower heating efficiency. On the other hand, in the "orbit improved" configuration, no saturation of the stored energy can be seen in Fig. 5-(b) because of the good heating efficiency. The fraction of the stored energies of the tail ions are more than 30% at the heating power of 10MW and still increases in the higher energy region.

Figure 6 shows the energy confinement time as a function of RF input power in the LHD, where the global energy confinement time (solid line), the slowing down time (dashed line), and the energy confinement time without tail effect (dotted line) are plotted. The plasma parameters are $n = 0.6 \times 10^{20}\mathrm{m}^{-3}$ and $B = 3.0T$.

The heating efficiency is almost unity with the low RF input power ($\lesssim$ 4MW) and slight increment from the simple LHD scaling is observed due to the tail effect in the the "standard" configuration in Fig. 6-(a). The slowing down time is so smaller than the energy confinement time that increment due to the tail effect is small. When the input power is increased, the decrease of the energy confinement time from the value of simple LHD scaling without tail effect is found due to the reduction of heating efficiency. On the other hand, in the "orbit improved" configuration the increment of energy confinement time form the LHD scaling can be seen in Fig. 6-(b).

Figure 7 shows the global energy confinement time versus the energy confinement time evaluated by LHD scaling. It is found that the systematic decrement of energy confinement time can be seen in the "standard" configuration and no density dependence can be seen. This tendency is very similar as that of CHS (See Fig. 3). On the other hand, the increment of

energy confinement time can be seen in the "orbit improved" configuration. Also we find that the increment of the energy confinement time depends on the density and the increment is higher for the lower density case.

5 Conclusions

We have investigated the ICRF heating efficiency and the global energy confinement for ICRF heated plasma including the effects of energetic ion loss in heliotrons. In order to consider the confinement of energetic tail ions and bulk plasma separately we have derived the formula of global energy confinement time as a function of the ICRF heating efficiency, the slowing down time, and the energy confinement time for bulk plasma, where the ICRF heating efficiency is defined by the fraction of the transferred power from energetic tail ions to bulk plasma to the absorbed ICRF heating power. Assuming the power balance of energetic ions the approximate formula of the heating efficiency is obtained based on the results of Monte Carlo simulations. Then the global energy confinement time can be estimated combining the heating efficiency with the energy confinement time of bulk plasma and the slowing down time of energetic ions.

The obtained formula has been applied to the ICRF minority heating in the CHS plasma. The ratio of the slowing down time to the energy confinement time is about 0.2 to 0.3 for the CHS plasma parameter. Since the confinement property of the energetic ions is not so optimized in CHS, the reduction of energy confinement due to energetic ion loss occurs in the heating power region ($P > 300$kW) rather than the increment by energetic ions. The global energy confinement time is systematically lower than the empirical scaling, and the difference becomes smaller for the combining heating case with direct electron heating. This result is consistent with the experimental results in CHS[1].

We have also applied our model to the ICRF minority heating in the LHD plasma in two cases of typical magnetic configurations. The reduction of the global energy confinement time from the LHD scaling is observed in the "standard" configuration. On the other hand, the increment of the energy confinement time can be seen in the "orbit improved" configuration. The density dependence of the increment also has been observed.

In this paper, the numeral power factors in the heating efficiency formula in the CHS and LHD plasmas are estimated by the results of Monte Carlo simulations, where we have ignored effects due to finite beta configurations. To take into account these effects and theoretically understand the values of these power factors are our future works.

Acknowledgments

The authors wish to thank Profs. T. Watari, T. Mutoh, R. Kumazawa and K. Nishimura for useful discussions. Members of ICRF heating Group and CHS Group at the National Institute for Fusion science are also acknowledged.

References

[1] NISHIMURA, K., et al., in Plasma Physics Controlled Nuclear Fusion Research 1994 (Proc. 15th Int. Conf. Seville, 1994), Vol. 1, IAEA, Vienna (1995) 679.

[2] MASUDA, S., et al., Nucl. Fusion **37** (1997) 53.

[3] MUTOH, T, et al., Nucl. Fusion **24** (1984) 1003.

[4] OKADA, H., et al., Nucl. Fusion **36** (1996) 465.

[5] NOTERDAEME, J.-M., et al., in Fusion Energy 1996 (Proc. 16th Int. Conf. Montreal, 1996) Vol. 3, IAEA, Vienna (1997) 335.

[6] HARTMANN, D.A., et al., Contr. Fusion Plasma Phys., Proc. 24th EPS Conf., Berchtesgaden (Germany, 1997) p1633.

[7] KWON, M., et al., Nucl. Fusion **32** (1992) 1225.

[8] JET TEAM, in Plasma Physics and Controlled Nuclear Fusion Research 1988 (Proc. 12th Int. Conf. Nice, 1998), Vol. 1, IAEA, Vienna (1989) 247.

[9] KIMURA, H., et al., Nuclear Fusion **31** (1991) 83.

[10] YAMAGIWA, M., et al., Plasma Phys. Cont. Fusion **30** (1988) 943.

[11] SUDO, S., et al., Nucl. Fusion **30** (1990) 11.

[12] MURAKAMI, S., et al., Nucl. Fusion **34** (1994) 913.

[13] MURAKAMI, S., et al., Fusion Eng. Design **26** (1995) 209.

[14] MURAKAMI, S., et al., in Plasma Physics and Controlled Nuclear Fusion Research 1994 (Proc. 15th Int. Conf. Sevilla, 1994), Vol. 3, IAEA, Vienna (1995) 531.

[15] ITHO, K., et al., Nucl. Fusion **28** (1988) 779.

[16] FUJIWARA, M., et al., J. Fusion Energy **15** (1996) 7.

[17] MURAKAMI, S., Annual Rep. NIFS 1994 (1995) p122.

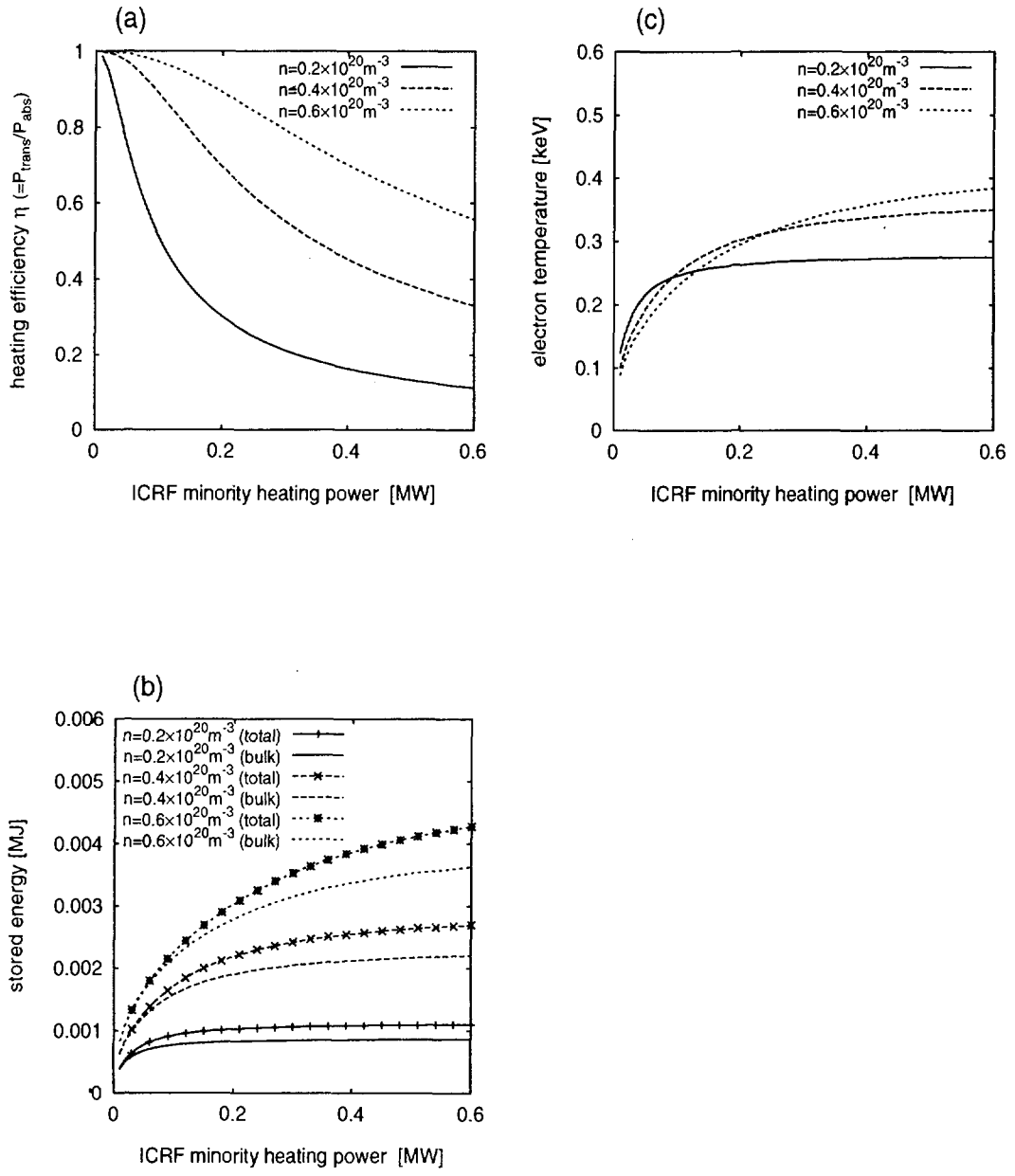

Fig. 1 : Plots of (a) the heating efficiencies, (b) the stored energies in the total and bulk plasma, and (c) the electron temperature in the CHS plasma(ICRF minority heating) as a function of heating power with three different densities $n = 0.2$, 0.4 and 0.6 $\times 10^{20}\mathrm{m}^{-3}$. The 10% of the minority fraction is assumed and the magnetic field strength is $B = 0.9\mathrm{T}$.

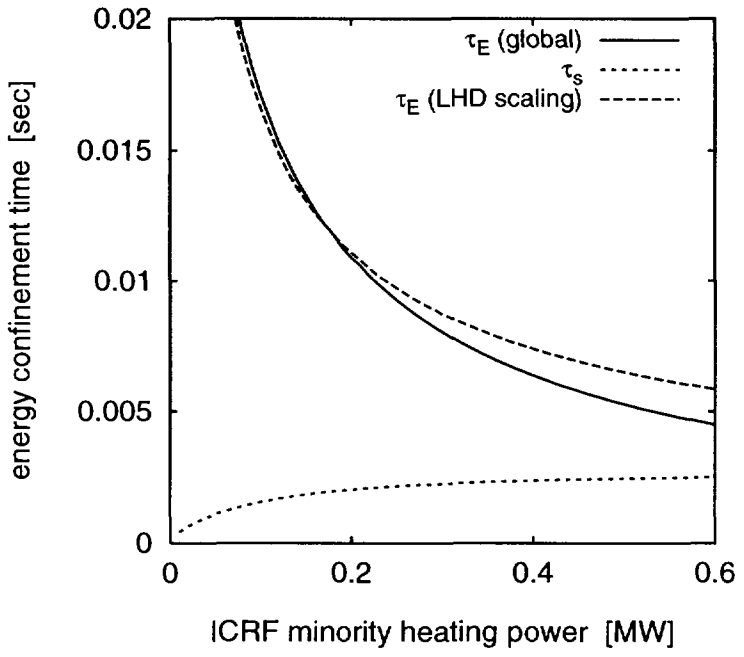

Fig. 2 : Plot of the calculated global energy confinement time including the energetic ion effect (solid line) in comparisons with the value estimated by LHD scaling law (dashed line) and the slowing down time of energetic ions in the CHS plasma (dotted line); $n = 0.6 \times 10^{20}\mathrm{m}^{-3}$ and $B = 0.9\mathrm{T}$

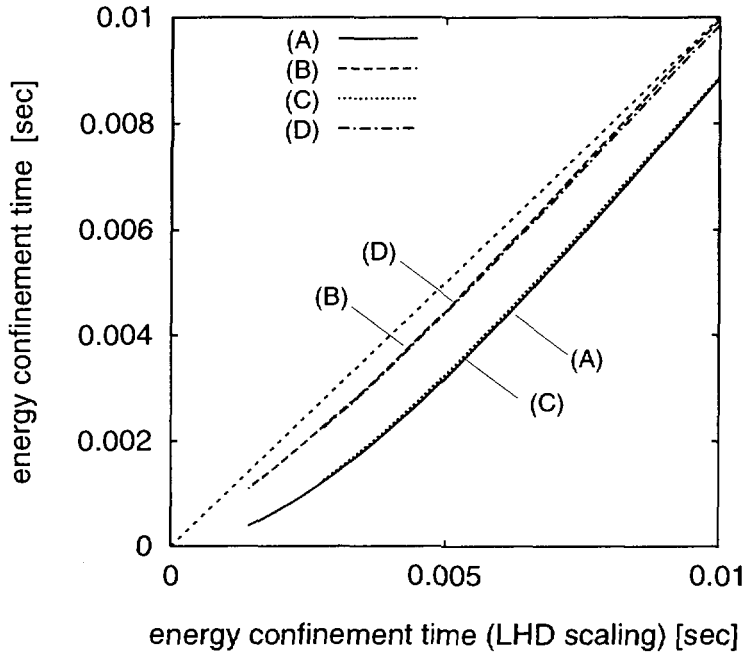

Fig. 3 : The global energy confinement time versus the energy confinement time by the LHD scaling law for two different plasma densities and heating scenarios in the CHS plasma; (A) only ion heating at $n = 0.15 \times 10^{20}\mathrm{m}^{-3}$, (B) ion and direct electron heating with equal weight at $n = 0.15 \times 10^{20}\mathrm{m}^{-3}$, (C) only ion heating at $n = 0.4 \times 10^{20}\mathrm{m}^{-3}$ and (D) ion and electron heating with equal weight at $n = 0.4 \times 10^{20}\mathrm{m}^{-3}$.

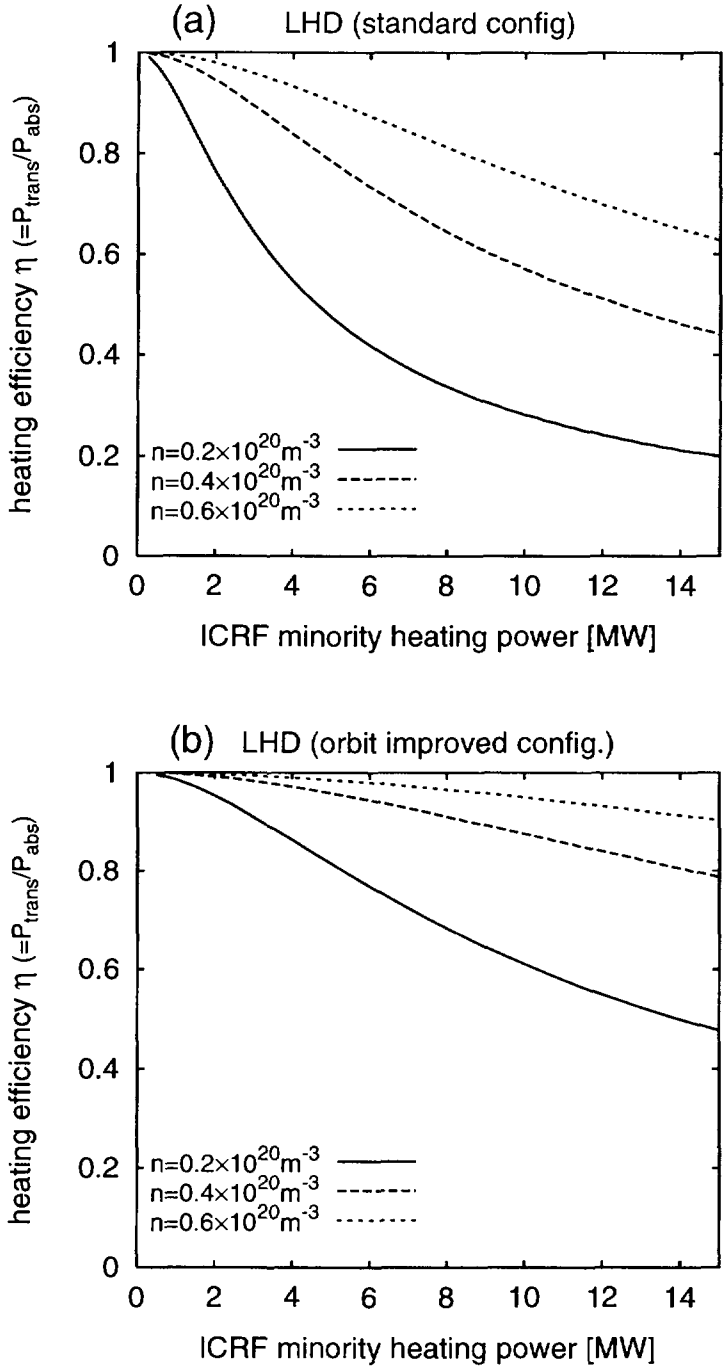

Fig. 4 : Plots of the heating efficiency as a function of the ICRF minority heating power for two different configurations of LHD; (a) "standard" configuration and (b) "orbit improved" configuration. The magnetic field strength is $B = 3$T and ^{3}He minority ions (3%) is assumed in deuteron plasma.

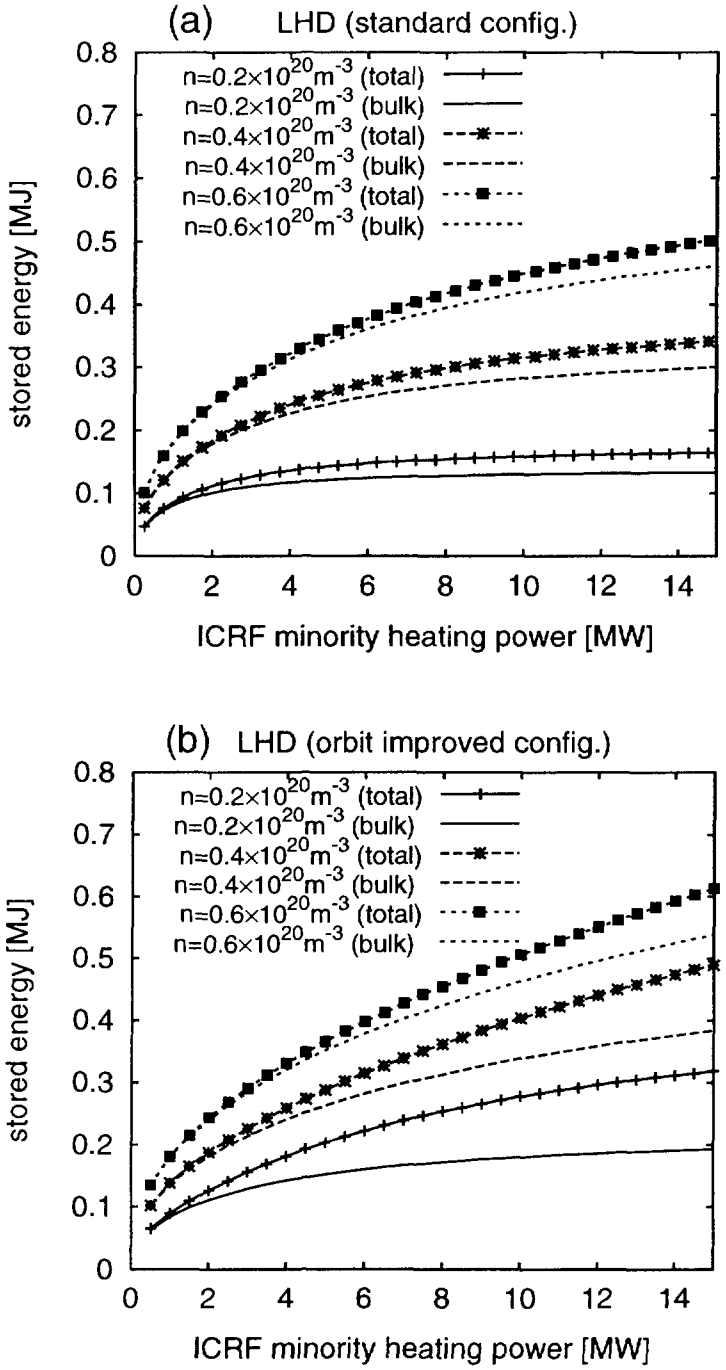

Fig. 5 : Plots of the stored energies in the total and bulk plasma as a function of the ICRF minority heating power for two different configurations of LHD; (a) "standard" configuration and (b) "orbit improved" configuration. The magnetic field strength is $B = 3\mathrm{T}$ and $^3\mathrm{He}$ minority ions (3%) is assumed in deuteron plasma.

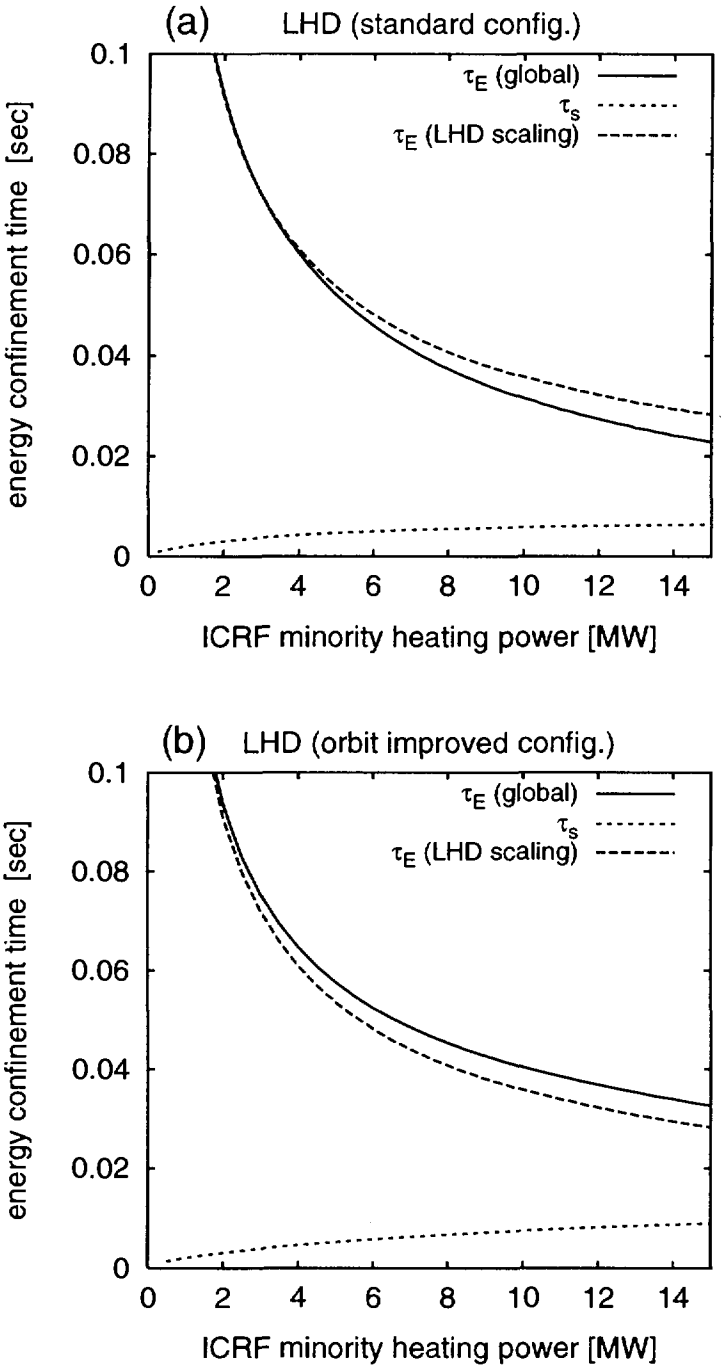

Fig. 6 : Plots of the calculated global energy confinement time (solid line) in comparison with the values estimated by LHD scaling law (dashed line) and the slowing down time (dotted line) for two different configurations of LHD; (a) "standard" configuration and (b) "orbit improved" configuration. ^{3}He minority ions (3%) is assumed in deuteron plasma, and the density and the magnetic field strength are $n = 0.6 \times 10^{20}\mathrm{m}^{-3}$ and $B = 3.0\mathrm{T}$, respectively.

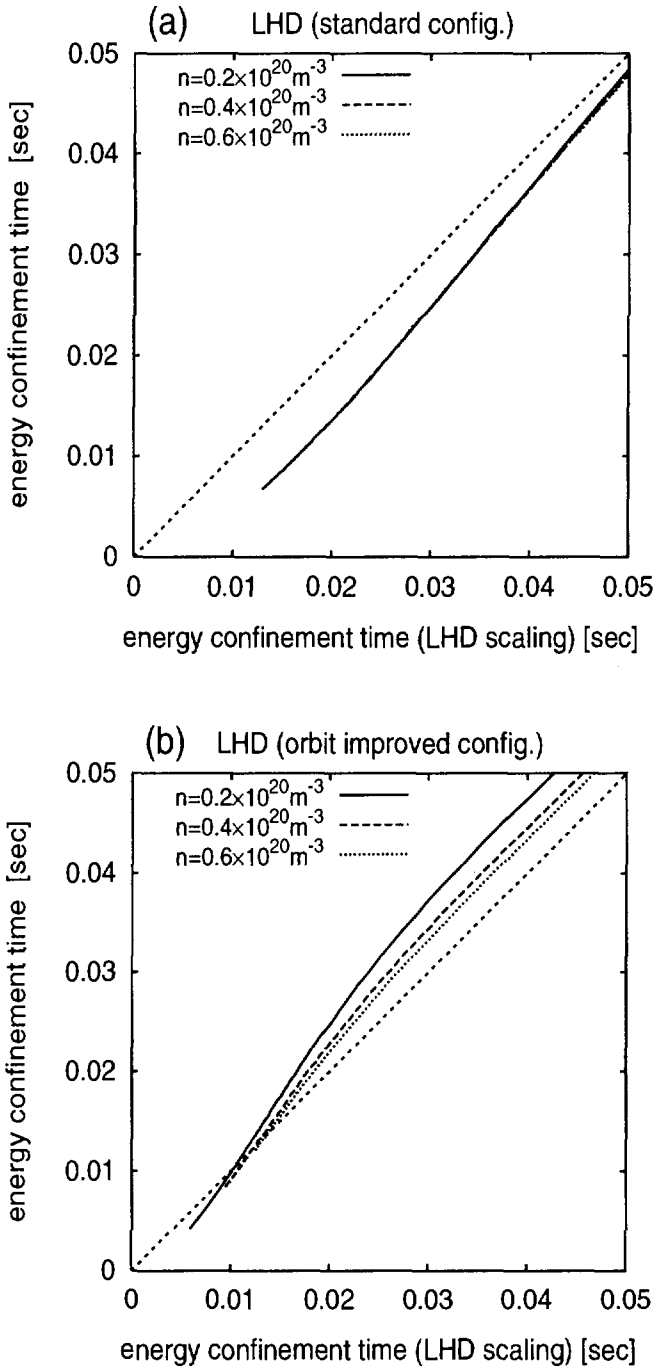

Fig. 7 : The global energy confinement time versus the energy confinement time by the LHD scaling law for two different configurations of LHD; (a) "standard" configuration and (b) "orbit improved" configuration. ^{3}He minority ions (3%) is assumed in deuteron plasma and the density and the magnetic field strength are $n = 0.6 \times 10^{20}\mathrm{m}^{-3}$ and $B = 3.0\mathrm{T}$, respectively.

Recent Issues of NIFS Series

NIFS-535 A. Fujisawa, H. Iguchi, H. Idei, S. Kubo, K. Matsuoka, S. Okamura, K. Tanaka, T. Minami, S. Ohdachi, S. Morita, H. Zushi, S. Lee, M. Osakabe, R. Akiyama, Y. Yoshimura, K. Toi, H. Sanuki, K. Itoh, A. Shimizu, S. Takagi, A. Ejiri, C. Takahashi, M. Kojima, S. Hidekuma, K. Ida, S. Nishimura, N. Inoue, R. Sakamoto, S.-I. Itoh, Y. Hamada, M. Fujiwara,
Discovery of Electric Pulsation in a Toroidal Helical Plasma; Jan. 1998

NIFS-536 Lj.R. Hadzievski, M.M. Skoric, M. Kono and T. Sato,
Simulation of Weak and Strong Langmuir Collapse Regimes; Jan. 1998

NIFS-537 H. Sugama, W. Horton,
Nonlinear Electromagnetic Gyrokinetic Equation for Plasmas with Large Mean Flows; Feb. 1998

NIFS-538 H. Iguchi, T.P. Crowley, A. Fujisawa, S. Lee, K. Tanaka, T. Minami, S. Nishimura, K. Ida, R. Akiyama, Y. Hamada, H., Idei, M. Isobe, M. Kojima, S. Kubo, S. Morita, S. Ohdachi, S. Okamura, M. Osakabe, K. Matsuoka, C. Takahashi and K. Toi,
Space Potential Fluctuations during MHD Activities in the Compact Helical System (CHS); Feb. 1998

NIFS-539 Takashi Yabe and Yan Zhang,
Effect of Ambient Gas on Three-Dimensional Breakup in Coronet Formation Process; Feb. 1998

NIFS-540 H. Nakamura, K. Ikeda and S. Yamaguchi,
Transport Coefficients of InSb in a Strong Magnetic Field; Feb. 1998

NIFS-541 J. Uramoto,
Development of ν_μ Beam Detector and Large Area ν_μ Beam Source by H_2 Gas Discharge (I); Mar. 1998

NIFS-542 J. Uramoto,
Development of $bar{\nu}_\mu$ Beam Detector and Large Area $bar{\nu}_\mu$ Beam Source by H_2 Gas Discharge (II); Mar. 1998

NIFS-543 J. Uramoto,
Some Problems inside a Mass Analyzer for Pions Extracted from a H_2 Gas Discharge; Mar. 1998

NIFS-544 J. Uramoto,
Simplified ν_μ, $bar{\nu}_\mu$ Beam Detector and ν_μ, $bar{\nu}_\mu$ Beam Source by Interaction between an Electron Bunch and a Positive Ion Bunch; Mar. 1998

NIFS-545 J. Uramoto,
Various Neutrino Beams Generated by D_2 Gas Discharge; Mar. 1998

NIFS-546 R. Kanno, N. Nakajima, T. Hayashi and M. Okamoto,
Computational Study of Three Dimensional Equilibria with the Bootstrap Current; Mar. 1998

NIFS-547 R. Kanno, N. Nakajima and M. Okamoto,
Electron Heat Transport in a Self-Similar Structure of Magnetic Islands; Apr. 1998

NIFS-548 J.E. Rice,
Simulated Impurity Transport in LHD from MIST; May 1998

NIFS-549 M.M. Skoric, T. Sato, A.M. Maluckov and M.S. Jovanovic,
On Kinetic Complexity in a Three-Wave Interaction; June 1998

NIFS-550 S. Goto and S. Kida,
Passive Scalar Spectrum in Isotropic Turbulence: Prediction by the Lagrangian Direct-interaction Approximation; June 1998

NIFS-551 T. Kuroda, H. Sugama, R. Kanno, M. Okamoto and W. Horton,
Initial Value Problem of the Toroidal Ion Temperature Gradient Mode; June 1998

NIFS-552 T. Mutoh, R. Kumazawa, T. Seki, F. Simpo, G. Nomura, T. Ido and T. Watari,
Steady State Tests of High Voltage Ceramic Feedthoughs and Co-Axial Transmission Line of ICRF Heating System for the Large Helical Device; June 1998

NIFS-553 N. Noda, K. Tsuzuki, A. Sagara, N. Inoue, T. Muroga,
oronaization in Future Devices -Protecting Layer against Tritium and Energetic Neutrals-: July 1998

NIFS-554 S. Murakami and H. Saleem,
Electromagnetic Effects on Rippling Instability and Tokamak Edge Fluctuations; July 1998

NIFS-555 H. Nakamura, K. Ikeda and S. Yamaguchi,
Physical Model of Nernst Element; Aug. 1998

NIFS-556 H. Okumura, S. Yamaguchi, H. Nakamura, K. Ikeda and K. Sawada,
Numerical Computation of Thermoelectric and Thermomagnetic Effects; Aug. 1998

NIFS-557 Y. Takeiri, M. Osakabe, K. Tsumori, Y. Oka, O. Kaneko, E. Asano, T. Kawamoto, R. Akiyama and M. Tanaka,
Development of a High-Current Hydrogen-Negative Ion Source for LHD-NBI System; Aug.1998

NIFS-558 M. Tanaka, A. Yu Grosberg and T. Tanaka,
Molecular Dynamics of Structure Organization of Polyampholytes: Sep. 1998

NIFS-559 R. Horiuchi, K. Nishimura and T. Watanabe,
Kinetic Stabilization of Tilt Disruption in Field-Reversed Configurations; Sep. 1998
(IAEA-CN-69/THP1/11)

NIFS-560 S. Sudo, K. Kholopenkov, K. Matsuoka, S. Okamura, C. Takahashi, R. Akiyama, A. Fujisawa, K. Ida, H. Idei, H. Iguchi, M. Isobe, S. Kado, K. Kondo, S. Kubo, H. Kuramoto, T. Minami, S. Morita, S. Nishimura, M. Osakabe, M. Sasao, B. Peterson, K. Tanaka, K. Toi and Y. Yoshimura,
Particle Transport Study with Tracer-Encapsulated Solid Pellet Injection: Oct. 1998
(IAEA-CN-69/EXP1/18)

NIFS-561 A. Fujisawa, H. Iguchi, S. Lee, K. Tanaka, T. Minami, Y. Yoshimura, M. Osakabe, K. Matsuoka, S. Okamura, H. Idei, S. Kubo, S. Ohdachi, S. Morita, R. Akiyama, K. Toi, H. Sanuki, K. Itoh, K. Ida, A. Shimizu, S. Takagi, C. Takahashi, M. Kojima, S. Hidekuma, S. Nishimura, M. Isobe, A. Ejiri, N. Inoue, R. Sakamoto, Y. Hamada and M. Fujiwara,
Dynamic Behavior Associated with Electric Field Transitions in CHS Heliotron/Torsatron: Oct. 1998
(IAEA-CN-69/EX5/1)

NIFS-562 S. Yoshikawa,
Next Generation Toroidal Devices; Oct. 1998

NIFS-563 Y. Todo and T. Sato,
Kinetic-Magnetohydrodynamic Simulation Study of Fast Ions and Toroidal Alfvén Eigenmodes; Oct. 1998
(IAEA-CN-69/THP2/22)

NIFS-564 T. Watari, T. Shimozuma, Y. Takeiri, R. Kumazawa, T. Mutoh, M. Sato, O. Kaneko, K. Ohkubo, S. Kubo, H. Idei, Y. Oka, M. Osakabe, T. Seki, K. Tsumori, Y. Yoshimura, R. Akiyama, T. Kawamoto, S. Kobayashi, F. Shimpo, Y. Takita, E. Asano, S. Itoh, G. Nomura, T. Ido, M. Hamabe, M. Fujiwara, A. Iiyoshi, S. Morimoto, T. Bigelow and Y.P. Zhao,
Steady State Heating Technology Development for LHD: Oct. 1998
(IAEA-CN-69/FTP/21)

NIFS-565 A. Sagara, K.Y. Watanabe, K. Yamazaki, O. Motojima, M. Fujiwara, O. Mitarai, S. Imagawa, H. Yamanishi, H. Chikaraishi, A. Kohyama, H. Matsui, T. Muroga, T. Noda, N. Ohyabu, T. Satow, A.A. Shishkin, S. Tanaka, T. Terai and T. Uda,
LHD-Type Compact Helical Reactors; Oct. 1998
(IAEA-CN-69/FTP/03(R)

NIFS-566 N. Nakajima, J. Chen, K. Ichiguchi and M. Okamoto,
Global Mode Analysis of Ideal MHD Modes in L=2 Heliotron/Torsatron Systems; Oct. 1998
(IAEA-CN-69/THP1/08)

NIFS-567 K. Ida, M. Osakabe, K. Tanaka, T. Minami, S. Nishimura, S. Okamura, A. Fujisawa, Y. Yoshimura, S. Kubo, R. Akiyama, D.S.Darrow, H. Idei, H. Iguchi, M. Isobe, S. Kado, T. Kondo, S. Lee, K. Matsuoka, S. Morita, I. Nomura, S. Ohdachi, M. Sasao, A. Shimizu, K. Tumori, S. Takayama, M. Takechi, S. Takagi, C. Takahashi, K. Toi and T. Watari,
Transition from L Mode to High Ion Temperature Mode in CHS Heliotron/Torsatron Plasmas; Oct. 1998
(IAEA-CN-69/EX2/2)

NIFS-568 S. Okamura, K. Matsuoka, R. Akiyama, D.S. Darrow, A. Ejiri, A. Fujisawa, M. Fujiwara, M. Goto, K. Ida H. Idei, H. Iguchi, N. Inoue, M. Isobe, K. Itoh, S. Kado, K. Khlopenkov, T. Kondo, S. Kubo, A. Lazaros, S. Lee, G. Matsunaga, T. Minami, S. Morita, S. Murakami, N. Nakajima, N. Nikai, S. Nishimura, I. Nomura, S. Ohdachi, K. Ohkuni, M. Osakabe, R. Pavlichenko, B. Peterson, R. Sakamoto, H. Sanuki, M. Sasao, A. Shimizu, Y. Shirai, S. Sudo, S. Takagi, C. Takahashi, S. Takayama, M. Takechi, K. Tanaka, K. Toi, K. Yamazaki, Y. Yoshimura and T. Watari,
Confinement Physics Study in a Small Low-Aspect-Ratio Helical Device CHS: Oct. 1998

(IAEA-CN-69/OV4/5)

NIFS-569 M.M. Skoric, T. Sato, A. Maluckov, M.S. Jovanovic,
Micro- and Macro-scale Self-organization in a Dissipative Plasma: Oct. 1998

NIFS-570 T. Hayashi, N. Mizuguchi, T-H. Watanabe, T. Sato and the Complexity Simulation Group,
Nonlinear Simulations of Internal Reconnection Event in Spherical Tokamak: Oct. 1998
(IAEA-CN-69/TH3/3)

NIFS-571 A. Iiyoshi, A. Komori, A. Ejiri, M. Emoto, H. Funaba, M. Goto, K. Ida, H. Idei, S. Inagaki, S. Kado, O. Kaneko, K. Kawahata, S. Kubo, R. Kumazawa, S. Masuzaki, T. Minami, J. Miyazawa, T. Morisaki, S. Morita, S. Murakami, S. Muto, T. Muto, Y. Nagayama, Y. Nakamura, H. Nakanishi, K. Narihara, K. Nishimura, N. Noda, T. Kobuchi, S. Ohdachi, N. Ohyabu, Y. Oka, M. Osakabe, T. Ozaki, B.J. Peterson, A. Sagara, S. Sakakibara, R. Sakamoto, H. Sasao, M. Sasao, K. Sato, M. Sato, T. Seki, T. Shimozuma, M. Shoji, H. Suzuki, Y. Takeiri, K. Tanaka, K. Toi, T. Tokuzawa, K. Tsumori, I. Yamada, H. Yamada, S. Yamaguchi, M. Yokoyama, K.Y.Watanabe, T. Watari, R. Akiyama, H. Chikaraishi, K. Haba, S. Hamaguchi, S. Iima, S. Imagawa, N. Inoue, K. Iwamoto, S. Kitagawa, Y. Kubota, J. Kodaira, R. Maekawa, T. Mito, T. Nagasaka, A. Nishimura, Y. Takita, C. Takahashi, K. Takahata, K. Yamauchi, H. Tamura, T. Tsuzuki, S. Yamada, N. Yanagi, H. Yonezu, Y. Hamada, K. Matsuoka, K. Murai, K. Ohkubo, I. Ohtake, M. Okamoto, S. Sato, T. Satow, S. Sudo, S. Tanahashi, K. Yamazaki, M. Fujiwara and O. Motojima,
An Overview of the Large Helical Device Project: Oct. 1998
(IAEA-CN-69/OV1/4)

NIFS-572 M. Fujiwara, H. Yamada, A. Ejiri, M. Emoto, H. Funaba, M. Goto, K. Ida, H. Idei, S. Inagaki, S. Kado, O. Kaneko, K. Kawahata, A. Komori, S. Kubo, R. Kumazawa, S. Masuzaki, T. Minami, J. Miyazawa, T. Morisaki, S. Morita, S. Murakami, S. Muto, T. Muto, Y. Nagayama, Y. Nakamura, H. Nakanishi, K. Narihara, K. Nishimura, N. Noda, T. Kobuchi, S. Ohdachi, N. Ohyabu, Y. Oka, M. Osakabe, T. Ozaki, B. J. Peterson, A. Sagara, S. Sakakibara, R. Sakamoto, H. Sasao, M. Sasao, K. Sato, M. Sato, T. Seki, T. Shimozuma, M. Shoji, H. Sazuki, Y. Takeiri, K. Tanaka, K. Toi, T. Tokuzawa, K. Tsumori, I. Yamada, S. Yamaguchi, M. Yokoyama, K.Y. Watanabe, T. Watari, R. Akiyama, H. Chikaraishi, K. Haba, S. Hamaguchi, M. Iima, S. Imagawa, N. Inoue, K. Iwamoto, S. Kitagawa, Y. Kubota, J. Kodaira, R. Maekawa, T. Mito, T. Nagasaka, A. Nishimura, Y. Takita, C. Takahashi, K. Takahata, K. Yamauchi, H. Tamura, T. Tsuzuki, S. Yamada, N. Yanagi, H. Yonezu, Y. Hamada, K. Matsuoka, K. Murai, K. Ohkubo, I. Ohtake, M. Okamoto, S. Sato, T. Satow, S. Sudo, S. Tanahashi, K. Yamazaki, O. Motojima and A. Iiyoshi,
Plasma Confinement Studies in LHD; Oct. 1998
(IAEA-CN-69/EX2/3)

NIFS-573 O. Motojima, K. Akaishi, H. Chikaraishi, H. Funaba, S. Hamaguchi, S. Imagawa, S. Inagaki, N. Inoue, A. Iwamoto, S. Kitagawa, A. Komori, Y. Kubota, R. Maekawa, S. Masuzaki, T. Mito, J. Miyazawa, T. Morisaki, T. Muroga, T. Nagasaka, Y. Nakmura, A. Nishimura, K. Nishimura, N. Noda, N. Ohyabu, S. Sagara, S. Sakakibara, R. Sakamoto. S. Satoh, T. Satow, M. Shoji, H. Suzuki, K. Takahata, H. Tamura, K. Watanabe, H. Yamada, S. Yamada, S. Yamaguchi, K. Yamazaki, N. Yanagi, T. Baba, H. Hayashi, M. Iima, T. Inoue, S. Kato, T. Kato, T. Kondo, S. Moriuchi, H. Ogawa, I. Ohtake, K. Ooba, H. Sekiguchi, N. Suzuki. S. Takami, Y. Taniguchi, T. Tsuzuki, N. Yamamoto, K. Yasui, H. Yonezu, M. Fujiwara and A. Iiyoshi,
Progress Summary of LHD Engineering Design and Construction: Oct. 1998
(IAEA-CN-69/FT2/1)

NIFS-574 K. Toi, M. Takechi, S. Takagi, G. Matsunaga, M. Isobe, T. Kondo, M. Sasao, D.S. Darrow, K. Ohkuni, S. Ohdachi, R. Akiyama A. Fujisawa, M. Gotoh, H. Idei, K. Ida, H. Iguchi, S. Kado, M. Kojima, S. Kubo, S. Lee, K. Matsuoka, T. Minami, S. Morita, N. Nikai, S. Nishimura, S. Okamura, M. Osakabe, A. Shimizu, Y. Shirai, C. Takahashi, K. Tanaka, T. Watari and Y. Yoshimura,
Global MHD Modes Excited by Energetic Ions in Heliotron/Torsatron Plasmas: Oct. 1998
(IAEA-CN-69/EXP1/19)

NIFS-575 Y. Hamada, A. Nishizawa, Y. Kawasumi, A. Fujisawa, M. Kojima, K. Narihara, K. Ida, A. Ejiri, S. Ohdachi, K. Kawahata, K. Toi, K. Sato, T. Seki, H. Iguchi, K. Adachi, S. Hidekuma, S.Hirokura, K. Iwasaki, T. Ido, R. Kumazawa, H. Kuramoto, T. Minami, I.. Nomura, M. Sasao, K.N. Sato, T. Tsuzuki, I. Yamada and T. Watari,
Potential Turbulence in Tokamak Plasmas: Oct. 1998
(IAEA-CN-69/EXP2/14)

NIFS-576 S. Murakami, U. Gasparino, H. Idei, S. Kubo, H. Maassberg, N. Marushchenko, N. Nakajima, M. Romé and M. Okamoto,
5D Simulation Study of Suprathermal Electron Transport in Non-Axisymmetric Plasmas: Oct. 1998
(IAEA-CN-69/THP1/01)

NIFS-577 S. Fujiwara and T. Sato,
Molecular Dynamics Simulation of Structure Formation of Short Chain Molecules: Nov. 1998

NIFS-578 T. Yamagishi,
Eigenfunctions for Vlasov Equation in Multi-species Plasmas Nov. 1998

NIFS-579 M. Tanaka, A. Yu Grosberg and T. Tanaka,
Molecular Dynamics of Strongly-Coupled Multichain Coulomb Polymers in Pure and Salt Aqueous Solutions: Nov. 1998

NIFS-580 J. Chen, N. Nakajima and M. Okamoto,
Global Mode Analysis of Ideal MHD Modes in a Heliotron/Torsatron System: I. Mercier-unstable Equilibria: Dec. 1998

NIFS-581 M. Tanaka, A. Yu Grosberg and T. Tanaka,
Comparison of Multichain Coulomb Polymers in Isolated and Periodic Systems: Molecular Dynamics Study; Jan. 1999

NIFS-582 V.S. Chan and S. Murakami,
Self-Consistent Electric Field Effect on Electron Transport of ECH Plasmas; Feb. 1999

NIFS-583 M. Yokoyama, N. Nakajima, M. Okamoto, Y. Nakamura and M. Wakatani,
Roles of Bumpy Field on Collisionless Particle Confinement in Helical-Axis Heliotrons; Feb. 1999

NIFS-584 T.-H. Watanabe, T. Hayashi, T. Sato, M. Yamada and H. Ji,
Modeling of Magnetic Island Formation in Magnetic Reconnection Experiment; Feb. 1999

NIFS-585 R. Kumazawa, T. Mutoh, T. Seki, F. Shinpo, G. Nomura, T. Ido, T. Watari, Jean-Marie Noterdaeme and Yangping Zhao,
Liquid Stub Tuner for Ion Cyclotron Heating; Mar. 1999

NIFS-586 A. Sagara, M. Iima, S. Inagaki, N. Inoue, H. Suzuki, K. Tsuzuki, S. Masuzaki, J. Miyazawa, S. Morita, Y. Nakamura, N. Noda, B. Peterson, S. Sakakibara, T. Shimozuma, H. Yamada, K. Akaishi, H. Chikaraishi, H. Funaba, O. Kaneko, K. Kawahata, A. Komori, N. Ohyabu, O. Motojima, LHD Exp. Group 1, LHD Exp. Group 2,
Wall Conditioning at the Starting Phase of LHD; Mar. 1999

NIFS-587 T. Nakamura and T. Yabe,
Cubic Interpolated Propagation Scheme for Solving the Hyper-Dimensional Vlasov-Poisson Equation in Phase Space; Mar. 1999

NIFS-588 W.X. Wnag, N. Nakajima, S. Murakami and M. Okamoto,
An Accurate δf Method for Neoclassical Transport Calculation; Mar. 1999

NIFS-589 K. Kishida, K. Araki, S. Kishiba and K. Suzuki,
Local or Nonlocal? Orthonormal Divergence-free Wavelet Analysis of Nonlinear Interactions in Turbulence; Mar. 1999

NIFS-590 K. Araki, K. Suzuki, K. Kishida and S. Kishiba,
Multiresolution Approximation of the Vector Fields on T^3; Mar. 1999

NIFS-591 K. Yamazaki, H. Yamada, K.Y.Watanabe, K. Nishimura, S. Yamaguchi, H. Nakanishi, A. Komori, H. Suzuki, T. Mito, H. Chikaraishi, K. Murai, O. Motojima and the LHD Group,
Overview of the Large Helical Device (LHD) Control System and Its First Operation; Apr. 1999

NIFS-592 T. Takahashi and Y. Nakao,
Thermonuclear Reactivity of D-T Fusion Plasma with Spin-Polarized Fuel; Apr. 1999

NIFS-593 H. Sugama,
Damping of Toroidal Ion Temperature Gradient Modes; Apr. 1999

NIFS-594 Xiaodong Li,
Analysis of Crowbar Action of High Voltage DC Power Supply in the LHD ICRF System; Apr. 1999

NIFS-595 K. Nishimura, R. Horiuchi and T. Sato,
Drift-kink Instability Induced by Beam Ions in Field-reversed Configurations; Apr. 1999

NIFS-596 Y. Suzuki, T-H. Watanabe, T. Sato and T. Hayashi,
Three-dimensional Simulation Study of Compact Toroid Plasmoid Injection into Magnetized Plasmas; Apr. 1999

NIFS-597 H. Sanuki, K. Itoh, M. Yokoyama, A. Fujisawa, K. Ida, S. Toda, S.-I. Itoh, M. Yagi and A. Fukuyama,
Possibility of Internal Transport Barrier Formation and Electric Field Bifurcation in LHD Plasma; May 1999

NIFS-598 S. Nakazawa, N. Nakajima, M. Okamoto and N. Ohyabu,
One Dimensional Simulation on Stability of Detached Plasma in a Tokamak Divertor; June 1999

NIFS-599 S. Murakami, N. Nakajima, M. Okamoto and J. Nuhrenberg,
Effect of Energetic Ion Loss on ICRF Heating Efficiency and Energy Confinement Time in Heliotrons; June 1999